Volume 1 | Number 1 | Jan 2013 | Pages 1–100

Nanoscale

www.rsc.org/nanoscale

ROYAL SOCIETY OF CHEMISTRY

ROYAL SOCIETY OF CHEMISTRY

www.rsc.org/nanoscale

Nanoscale

ARTICLE

Seed-mediated growth of Au nanorings with size control on Pd ultrathin nanosheets and their tunable surface plasmonic properties

Wenxing Wang, Yucong Yan, Ning Zhou, Hui Zhang,* Dongsheng Li,* and Deren Yang

Nanorings made of noble metals such as Au and Ag have attracted particular interest in plasmonic properties since they allow remarkable tunability of plasmon resonance wavelengths associated with their unique structure features. Unfortunately, most of the syntheses for Au nanorings involve in the complex procedures and/or require highly specialized and expensive facilities. Here, we report a seed-mediated approach for selective deposition of Au nanorings on the periphery of Pd seeds with a structure of ultrathin nanosheet through island growth mode. In combination with selective etching of Pd nanosheets, Au nanorings are eventually produced. We can control the outer diameter and wall thickness of the nanorings by simply varying the size of Pd nanosheets and reaction time. By taking the advantage of this size controllability, the nanorings show the tunable surface plasmonic properties in a near infrared (NIR) region arising from both the in-plane dipole and face resonance modes. Owing to their good surface plasmonic properties, the nanorings show the substantially enhanced surface-enhanced Raman spectroscopy (SERS) performance for rhodamine 6G, which are therefore confirmed as good SERS substrates to detect trace amounts of molecules.

Introduction

Noble metal nanocrystals, especially for Au and Ag nanostructures, have been extensively studied in the past few decades for their potential use in surface enhanced Raman scattering (SERS), plasmonics, biosensing, photothermal therapy, and so forth.[1-7] Most of these applications rely on the unique optical properties of noble-metal nanostructures, that is, the localized surface plasmon resonance (LSPR), which originates from collective oscillation of their free electrons in response to an incident light at a certain frequency.[8-10] It is well-established that the plasmonic properties of noble-metal nanocrystals are highly dependent upon their size, shape, composition, interparticle distance, and dielectric environment.[11-13] Among them, controlling the shape of noble-metal nanocrystals offers promising opportunity to tune their LSPR properties with greater versatility including resonance mode, frequency, and intensity.[14-17] As such, there are strong efforts to maneuver the shape of noble-metal nanocrystals by exploiting a large number of synthetic approaches.[18] Taking Au

nanocrystals as examples, a rich varieties of shapes with solid interiors such as spheres, rods, plates, cubes, wires, concave cubes, and stars have been successfully generated by far.[19-27]

Recently, more interests are focused on the synthesis of Au nanocrystals with hollow interiors since such hollow nanostructures have a larger surface-to-volume ratio relative to solid counterpart, and thus exhibit enhanced interaction with light and surrounding media.[28] This strong interaction further yields intense local electromagnetic field enhancement in SERS with improved performance.[29] In addition, the strong coupling between charges on the outer and inner shells in a hollow structure can cause large charge separation, leading to the red shift of the LSPR peak.[30] As such, hollowing out a metal nanostructure is also a powerful means to tremendously expand the range of LSPR spectra in a longer wavelength and thus increase its applications in many aspects including SERS and biomedicine.[31-33] To this end, substantial research efforts have been employed to synthesize hollow Au nanostructures, with notable examples including hollow cages, rattles, frames, rings, etc.[34-38] Of them, Au nanorings are of particular interest because they allow significant tunability of LSPR properties associated with variable transverse and longitudinal axes.[39] Up to now, several synthetic methods including galvanic replacement, lithography, seed-mediated growth have been developed for the synthesis of Au nanorings with different shapes.[40-43] For instance, Xia and co-workers have demonstrated the synthesis of triangular Au nanorings through a galvanic replacement between triangular Ag nanoplates and

a. State Key Laboratory of Silicon Materials, School of Materials Science and Engineering, and Cyrus Tang Center for Sensor Materials and Applications, Zhejiang University, Hangzhou, Zhejiang 310027, P. R. China. FAX: +86-571-87952322; TEL: 86-571-87953190.
*Correspondence to: msezhanghui@zju.edu.cn, mselds@zju.edu.cn.
Electronic Supplementary Information (ESI) available: [details of any supplementary information available should be included here]. See DOI: 10.1039/x0xx00000x

aqueous $HAuCl_4$ solution.[44] In combination with Au overgrowth, the galvanic replacement was also used to synthesize the nanoprisms with a pore in the interior.[45] Since alloying process between Au and Ag co-exists in the galvanic replacement reaction, this approach has met serious limitation in the synthesis of pure Au nanorings. Several lithography techniques such as colloidal lithography, on-wire lithography, and electron beam lithography have been exploited to synthesize uniform and ordered Au nanorings.[46-49] However, these techniques usually suffer from the complicated and time-consuming procedures and require highly specialized and expensive facilities. Most recently, seed-mediated growth has emerged as a simple and powerful method for producing Au nanorings with two-dimensional (2D) nanocrystals as the seeds because of its relatively simple setup and high throughput. For example, Park and co-workers have reported the synthesis of 2D Pt@Au nanorings with high uniformity via site-selective growth of Pt serving Au nanodisks as the seeds, followed by etching and regrowth of Au.[50] Despite enormous success, size-controlled synthesis of Au nanorings with tunable plasmonic properties prepared by a facile and versatile method still remains a great challenge, especially for such nanorings with small outer diameters (e.g., < 50 nm) and thin wall thicknesses (e.g., < 10 nm).

Herein, we report a seed-mediated approach to the synthesis of Au nanorings by site selective growth of Au on the periphery of Pd ultrathin nanosheets. By varying the edge length of the Pd seeds and overgrowth time for Au, we can readily tune the size in terms of outer diameter and wall thickness of the Au nanorings. By taking the advantage of this size adjustability, such Au nanorings exhibit the tunable LSPR peaks located in the broad NIR region and show the substantially enhanced SERS signal for detecting rhodamine 6G (R6G).

Experimental Section

Chemicals and materials.

Palladium(II) acetylacetonate ($Pd(acac)_2$, 99%), L-ascorbic acid (AA, 99%), polyvinyl pyrrolidone (PVP, MW = 29000), tungsten hexacarbonyl ($W(CO)_6$, 97%) and rhodamine 6G (R6G) were purchased from Sigma-Aldrich. Hydrogen tetrachloroaurate (III) hydrate ($HAuCl_4·4H_2O$, 99%), citric acid (CA), cetyltrimethylammonium bromide (CTAB), N,N-dimethylformamide (DMF, AR), ethanol (AR), nitric acid (AR), and acetone (AR) were purchased from Sinopharm Chemical Reagent Co., Ltd. All the chemicals were used as received.

Synthesis of Pd nanosheets with different sizes.

Pd nanosheets with different sizes were synthesized by the reduction of Pd precursor in DMF containing CTAB, CA, and $W(CO)_6$ according to our previously reported method.[51,52] In a typical synthesis for Pd nanosheets with an average edge length of 18 nm, 16 mg of $Pd(acac)_2$, 90 mg of CA, 60 mg of CTAB, and 30 mg of PVP were dissolved into 10 mL of DMF and the mixed solution was stirred for 1 h. The obtained

homogeneous orange red solution was then transferred into a 25 mL flask and 100 mg of $W(CO)_6$ was added into the flask under Ar atmosphere. The flask was capped and heated at 80 °C for 1 h. After that, the Pd nanosheets were collected by centrifugation using a sufficient amount of acetone, and then re-dispersed in ethanol. This process was repeated three times. Pd nanosheets with average edge lengths of 28 and 38 nm were synthesized by varying the amount of CA to 50 and 20 mg, respectively.

Synthesis of Pd ultrathin nanosheet supported Au nanorings with different sizes.

In a standard synthesis, Pd ultrathin nanosheet supported Au nanorings with an average outer diameter of 38.3 nm were synthesized by dispersing 1.64 μmol of 18 nm Pd nanosheets, 200 mg of AA, and 200 mg of PVP into 3 mL of DMF and 2 mL of H_2O in a 25 mL flask. The flask was then immersed into an ice water bath to keep 0 °C. After that, 5 mL of $HAuCl_4$ with a concentration of 1.64 mM was added into the aforementioned mixture using a syringe pump at an injection rate of 1 mL/h for 5 h under magnetic stirring. The product was finally collected by centrifugation at 8000 rpm for 7 min and washed with acetone/alcohol for three times. The wall thickness and outer diameter of the nanorings were tuned by varying the reaction time and the size of the corresponding Pd seeds, respectively.

Synthesis of Au nanorings via chemical etching.

To remove the Pd nanosheets in the interior of the Au nanorings, 30 mg of PVP, 5 mL of HNO_3 solution with a concentration of 1 M and 2 mL of Pd nanosheet supported Au nanorings stock solution were added to a 20 mL vial. The mixture was then stirred at room temperature for 3 h. The final product was collected by centrifugation and washed with alcohol for three times.

Morphological, structural, and elemental characterizations.

Transmission electron microscopy (TEM) images were taken using a Hitachi HT-7700 microscope operated at 100 kV. High-resolution TEM (HRTEM) and high-angle annular dark-field scanning TEM (HAADF-STEM) were performed using a FEI Tecnai G2 F20 microscope operated at 200 kV. Energy dispersive X-ray spectroscopy (EDX) was performed using a Tecnai G2 F20 ChemiSTEM equipped with an Oxford X-Max 80T EDX detector system. X-ray powder diffraction (XRD) pattern was obtained by using a Rigaku D/MAX-ga X-ray diffractometer with graphite monochromatized Cu Kα radiation (λ = 1.54178 Å). Ultraviolet-visible-near infrared (UV-vis-NIR) extinction spectra were measured on a Maya2000 Pro Spectrophotometer over the range of 200-1100 nm by using ethanol as the solvent.

SERS measurements.

SERS spectra were recorded on a Raman spectrometer (Bruker Senterra) with an Ar^+ gas laser (532 nm). The laser power on the specimens was about 2 mW. The substrate for SERS was prepared by drying a 60 μL aliquot of the final product on a 50 nm thick Au film supported on a Si wafer. R6G was selected as a model analyte to investigate the performance of Pd

nanosheet supported Au nanorings. 25 µL of 10^{-6} M R6G ethanol solutions were dispersed on the as-prepared substrates and dried in an oven at 50 °C for SERS detection.
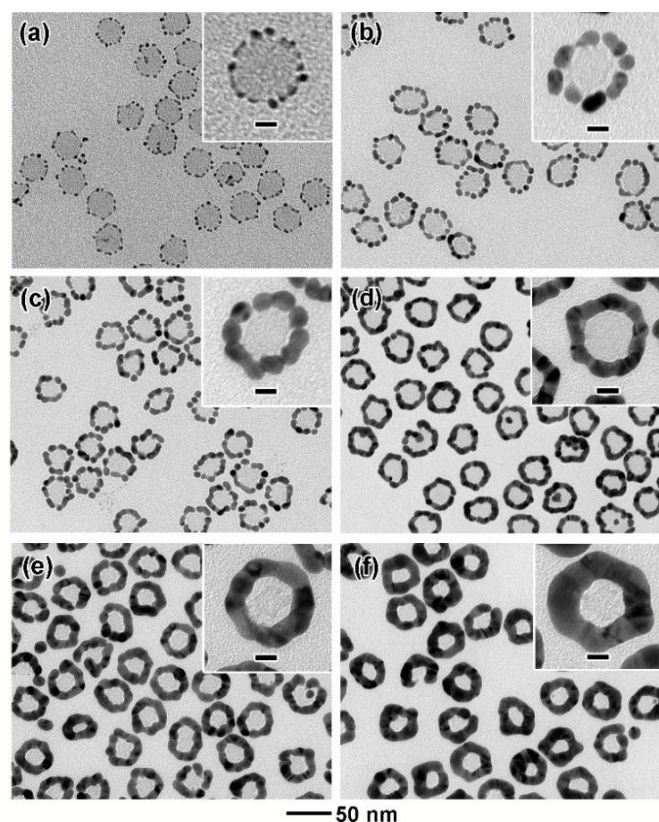
Results and discussion

Figure 1. TEM images of the samples prepared by injecting the Au precursor with an injection rate of 1 mL/h for different times: (a) 0.25, (b) 1, (c) 3 (d) 5, (e) 7, and (f) 9 h. The insets show the corresponding TEM images at a higher magnification. The scale bars in the insets are 10 nm.

The Pd nanosheet supported Au nanorings were generated by the reduction of $HAuCl_4$ with AA serving Pd ultrathin nanosheets as the seeds. The Pd hexagonal nanosheets have an average edge length of 18 nm (Figure S1). We monitored the growth of Au on the Pd nanosheets by imaging the products obtained at different reaction times. Figure 1 shows a series of TEM images taken from the samples that were obtained at different stages of a synthesis with an injection rate of 1 mL/h. In the initial stage of the reaction (Figure 1a, 0.25 mL of $HAuCl_4$ at t = 0.25 h), numerous Au nanoparticles were deposited preferentially on the periphery of the Pd nanosheets through an island growth mode. This island growth behavior can be attributed to the stronger bonding between Au-Au than Pd-Au, which is in agreement with the previous report.[53] The edges of the Pd nanosheets selectively act as the nucleation and growth sites of Au nanoparticles since these sites mainly enclosed by {100} facets have the higher surface energy relative to {111} planes.[54] Almost no isolated Au nanoparticles were observed in the TEM measurements, indicating the majority of the heterogeneous nucleation. The

magnified TEM image (inset of Figure 1a) shows that the size of the Au nanoparticles deposited on a Pd nanosheet is about 2-4 nm. As the amount of the Au precursor was increased to 1 mL (Figure 1b, t = 1 h), the as-preformed Au nanoparticles on the Pd nanosheets served as the seeds for subsequent growth of small nanoparticles into large ones with size of about 4-6 nm (inset of Figure 1b). As the reaction proceeded (Figure 1c, 3 mL at t = 3 h), the newly formed Au atoms were preferentially deposited in the gap between particles, resulting in the tendency to form the ring-like structures. After 5 mL of the precursor was added (Figure 1d, t = 5 h), these Au particles were gradually connected with each other and high-quality Au nanorings were eventually formed. The average outer diameter and wall thickness of the Au nanorings were measured to be 38.3 nm and 8.2 nm, respectively (Figure S2). The data were obtained from 100 nanocrystals randomly selected from TEM images. The size of the Au nanorings was further tuned by increasing the amount of the precursor fed in the synthesis, as shown in Figure 1, e and f. The statistical data in Figure S2 show that both the average outer diameter and wall thickness increased with increase of the amount of the Au precursor. A summary for the formation of the Pd ultrathin nanosheet supported Au nanorings is shown in Figure 2.
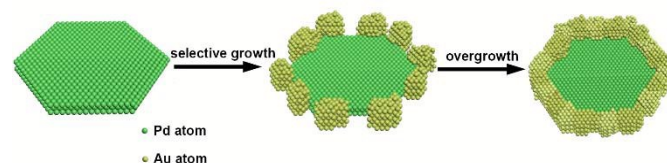

Figure 2. A schematic illustrating the formation mechanism of the Pd ultrathin nanosheet supported Au nanorings.

The growth of Au nanorings on the Pd nanosheets was also monitored by characterizing their LSPR properties using UV-vis-NIR spectroscopy. Typically, the Pd nanosheets with an average length of 18 nm exhibited a broad LSPR band centered at ~940 nm, which can be assigned to the in-plane dipole resonance of the hexagonal nanosheets (Figure S1b).[51] Figure 3 shows UV-vis-NIR extinction spectra of the samples that were obtained at different stages of the synthesis corresponding to the ones in Figure 1. As observed, the LSPR peak of the Pd nanosheets disappeared immediately once the Au nanoparticles were deposited on the surface of the Pd nanosheets (t = 0.25 h). This phenomenon is probably due to the surface plasmon coupling between the Au nanoparticles and Pd nanosheets. As the reaction proceeded, the samples exhibited the dramatic appearance of two distinct peaks that were centered at ~520 nm and a tunable wavelength range of 770-915 nm. According to the theoretical calculation,[39] the weak peak located at ~520 nm can be assigned to the out-of-plane dipole mode of the Au nanorings, which is influenced by the ring height. In addition, the strong resonance at NIR region originates from a combination of the in-plane dipole and face resonance modes in the nanorings, which is determined by both the outer diameter and wall thickness. During the overgrowth of Au, we found that a combination of the in-plane dipole and surface resonance modes has a blue-shift of about

145 nm from 915 to 770 nm in wavelength. The blue-shift in peak positions might be caused by the increase in wall thickness. However, the peak position for the out-of-plane dipole mode has a slight red-shift possibly owing to a little increase of the ring height during the synthesis. The ring height of the samples prepared at 5, 7, and 9 h is summarized in Figure S3. The ring height was measured by using carbon nanotubes as the support to allow the attachment of the rings vertically on the outer surface of the nanotubes (Figure S4). In addition, the intensity of these two resonance modes gradually increases with the extension of the reaction till the regular Au nanorings are formed at 5 h.
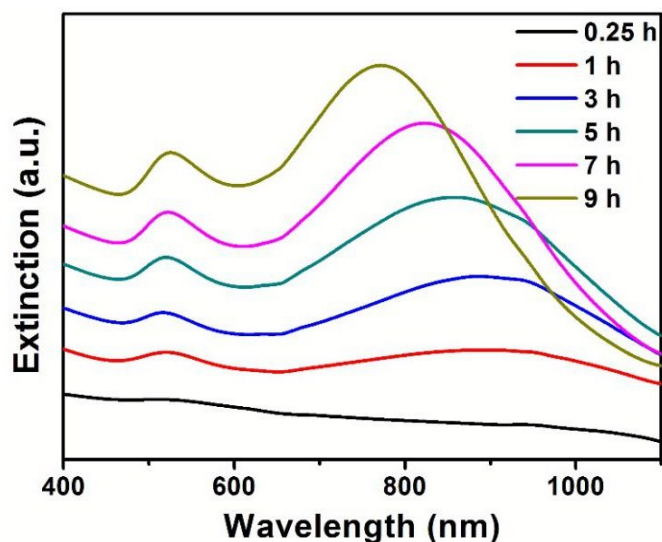

Figure 3. UV-vis-NIR extinction spectra of the Pd nanosheet supported Au nanorings prepared by injecting the Au precursor with an injection rate of 1 mL/h for different times. The samples correspond to those in figure 1.
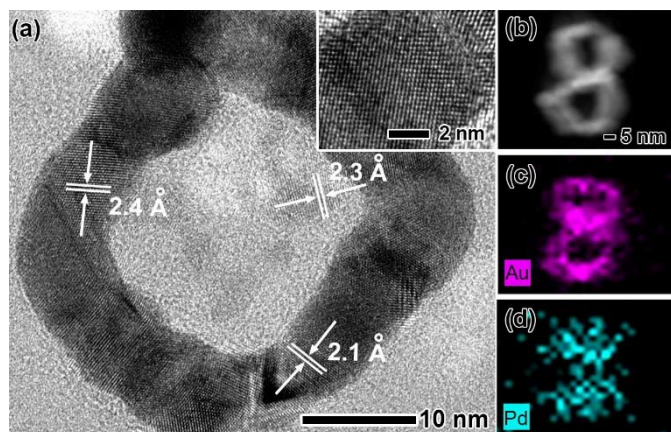

Figure 4. (a) HRTEM, (b) HAADF-STEM, and (c, d) EDX mapping images of the Pd nanosheet supported Au nanorings prepared using the standard procedure. The inset in (a) corresponds to a HRTEM image at a higher magnification. The purple and cyan colors in c and d correspond to Au and Pd elements, respectively.

Figure 4 shows HRTEM, HAADF-STEM, and EDX mapping images of the Pd nanosheets supported Au nanorings prepared using the standard procedure. From the HRTEM image in Figure 4a, the nanoring is composed of many

nanoparticles, indicating its polycrystalline structure. The magnified HRTEM image of an individual particle (inset of Figure 4a) shows well-resolved, continuous fringes with the same orientation, indicating that the particle is a single crystal. The fringes with the lattice spacing of 2.1 and 2.4 Å in the wall can be indexed to the {200} and {111} of Au with a *fcc* structure, respectively. While, the fringes with a lattice spacing of 2.3 Å at the central part can be indexed to the {111} planes of Pd. The ring-like structure is also confirmed by HAADF-STEM image, as shown in Figure 4b. EDX mapping analysis (Figure 4, c and d) shows that there are two elements in the sample: Pd and Au. Obviously, Pd came from the Pd ultrathin nanosheets in the interior, while Au originated from the Au nanorings in the exterior. This result indicates the successful synthesis of Pd nanosheet supported Au nanorings. XRD analysis of this sample (Figure S5a) clearly shows that the diffraction peaks can be indexed to Au with a *fcc* structure. There is almost no diffraction signal arising from Pd nanosheets due to their ultrathin thickness. For the production of pure Au nanorings, the Pd cores are selectively removed by chemical etching with an excess amount of HNO_3 at room temperature. From the TEM image in Figure 5a, well-defined Au nanorings with a hollow structure were obtained after chemical etching. This demonstration is also supported by HAADF-STEM-EDX mapping analysis (Figure 5, b-d). As observed, most of Pd cores were removed, while, Au was distributed throughout the entire nanoring, indicating the formation of the pure Au nanorings. XRD pattern in Figure S5b further confirms the nanorings made of Au with a *fcc* structure. The average outer diameter and wall thickness of the pure Au nanorings were measured to be 38.6 and 8.5 nm, respectively (Figure S6), which are almost the same as those of the sample before etching. In addition, we compare the LSPR properties of the Au nanorings before and after the removal of Pd nanosheets by chemical etching, as shown in Figure S7. There is a slight red-shift of about 30 nm in the in-plane resonance mode due to the removal of the Pd nanosheets.
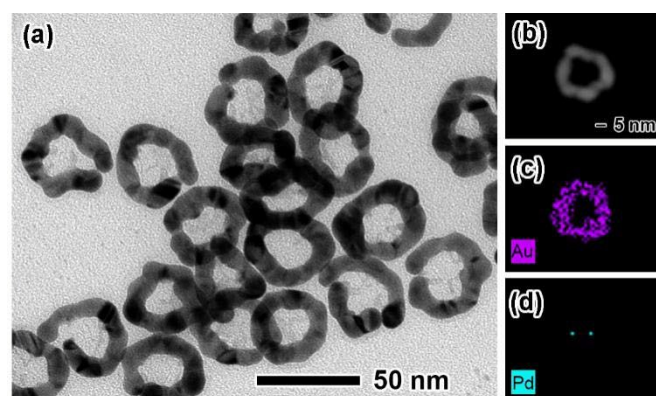

Figure 5. (a) TEM, (b) HAADF-STEM, and (c, d) EDX mapping images of the Au nanorings after chemical etching of the Pd nanosheets in the interior. The purple and cyan colors in (c) and (d) correspond to Au and Pd elements, respectively.

We also systematically investigated the effects of other important experimental parameters on the growth of the Pd nanosheets supported Au nanorings. In the standard

Journal Name ARTICLE

procedure except for the fast injection rate (e.g., 15 mL/h, Figure S8a), some isolated Au nanoparticles coexists with the nanorings due to the homogeneous nucleation. In addition, most of the nanorings have a gap in the wall probably due to the limited diffusion rate relative to the deposition rate (arising from fast injection rate).[55] When the reaction is conducted at relatively high temperature (e.g., 35 °C, Figure S8b), the nanorings are successfully generated. However, there are many isolated Au nanoparticles coexisted in the final product due to the homogeneous nucleation. Taken together, the injection rate and reaction temperature play important roles in facilitating the formation of the nanorings in high-quality.
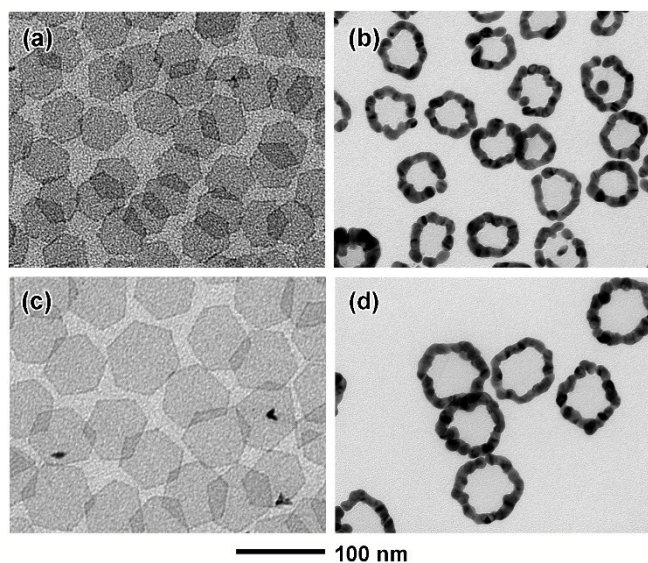

Figure 6. TEM images of the Pd nanosheets with an average edge length of (a) 28 and (c) 38 nm, respectively, and (b, d) their corresponding Pd nanosheet supported Au nanorings prepared using the Pd nanosheets as the seeds.
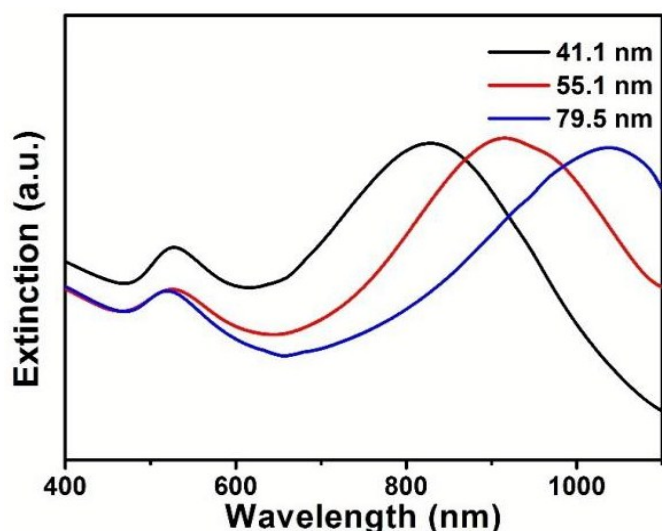

Figure 7. UV-vis-NIR extinction spectra of the Pd nanosheet supported Au nanorings with average outer diameters of 41.1, 55.1, and 79.5 nm, respectively.

We can simply control the size of the Au nanorings by choosing the Pd nanosheets with different edge lengths as the

seeds. Figure 6 shows TEM images of the Pd nanosheets with average edge lengths of 28 and 38 nm, respectively, together with the corresponding Au nanorings. From the statistical data in Figure S9, the outer diameter of the Au nanorings increases from 55.1 to 79.5 nm when varying the edge length of the Pd nanosheets from 28 to 38 nm. The wall thickness of these rings is mainly maintained. The Au nanorings exhibit size-dependent LSPR properties with highly tunable wavelength in NIR region. Figure 7 shows UV-vis-NIR extinction spectra of the Pd nanosheet supported Au nanorings by increasing the outer diameter, while, keeping the wall thickness constant. The peak positions in NIR region varied from 825 to 1040 nm by increasing the overall ring size. As well known, this red-shift with increase of the outer diameter can be attributed to the stronger charge separation on the nanorings and thus a lower frequency for the collective oscillation of electrons.[39] This tendency is consistent with the results of Au nanorings that were generated by on-wire lithography.[48]
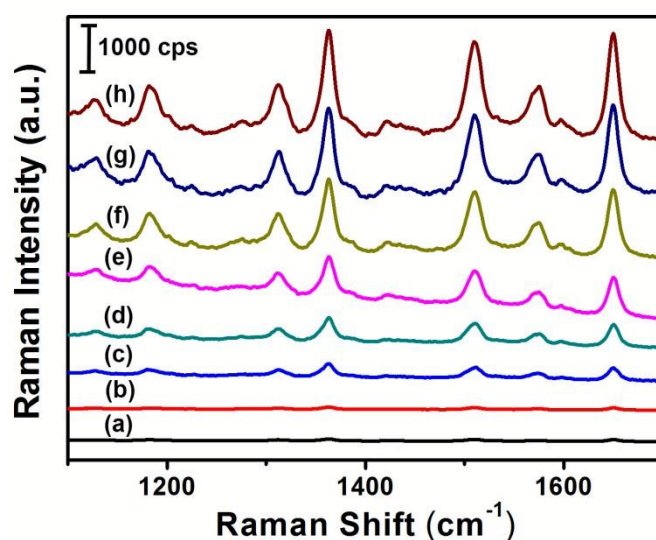

Figure 8. SERS spectra (cps=counts per second) of R6G on the different substrates. (a) blank sample (50 nm thick Au film supported on a Si wafer), (b) Pd nanosheets with an average edge length of 18 nm, Pd nanosheet supported Au nanorings prepared for different injection times (c) 0.25, (d) 1, (e) 3, and (f) 5 h, and Pd nanosheet supported Au nanorings with average outer diameters of (g) 51.1 and (h) 79.5 nm, respectively.

The Pd nanosheet supported Au nanorings were further evaluated as the substrate for SERS. We chose R6G as a probe molecule in our studies. Figure 8 compares the SERS activities of the Pd nanosheet supported Au nanorings prepared by varying the amount of Au precursor from 0.25 to 5 mL (Figure 1, a-d) and such nanorings with outer diameters of 55.1 and 79.5 nm, respectively. We benchmarked the SERS sensitivity of the Pd nanosheet supported Au nanorings against the blank sample and Pd nanosheets. In the blank sample (Figure 8a), no Raman signal of R6G is detected, showing the poor SERS sensitivity of R6G on Au film coated Si wafer. In the presence of the Pd nanosheets (Figure 8b), there is almost no Raman signal of R6G to be detected, indicating that the Pd nanosheets

are useless to obviously improve the SERS detecting. Once the Au nanoparticles were deposited on the Pd nanosheets, the Raman signal of R6G was dramatically enhanced due to the larger localized electric field (Figure 8c). In addition, this Raman signal gradually became stronger during the deposition of the Au nanoparticles till the regular Au nanorings were generated (Figure 8, d-f). This result is consistent with the variation in the LSPR intensity of these Pd nanosheet supported Au nanorings. Compared to the Pd nanosheets, the Au nanorings show the substantially enhanced SERS signal with a maximum enhancement of more than two thousand times. For the Au nanorings with larger sizes (Figure 8, g and h), there is no obvious difference in SERS signal, indicating that the size variation in this range has no great influence on the SERS properties.

Conclusions

In summary, we have demonstrated a facile and versatile approach for the synthesis of the Pd nanosheets supported Au nanorings with ultrathin Pd nanosheets as the seeds. After chemical etching of Pd nanosheets, the Au nanorings were successfully generated. We found that the key to the synthesis of the nanorings is the selective deposition of Au nanoparticles on the periphery of the Pd nanosheets through island growth mode. By varying the size of the nanorings (e.g., outer diameter and wall thickness), we can readily tune their LSPR properties in a broad region from 770 to 1040 nm. When evaluated as the substrate for SERS, such nanorings show remarkably improved SERS performance in detecting trace amounts of R6G compared to the Pd nanosheets due to the stronger resonance associated with the ring structure feature.

Acknowledgements

Notes and references

1. X. Qian, S. Nie, *Chem. Soc. Rev.*, 2008, **37**, 912-920.
2. Y. Yang, J. Liu, Z. Fu, D. Qin, *J. Am. Chem. Soc.*, 2014, **136**, 8153-8156.
3. J. Herzog, M. Knight, Y. Li, K. Evans, N. Halas, D. Natelson, *Nano Lett.,* 2013, **13**, 1359-1364.
4. N. Jiang, L. Shao, J. Wang, *Adv. Mater.,* 2014, **26**, 3282-3289.
5. C. Gao, Z. Lu, Y. Liu, Q. Zhang, M. Chi, Q. Cheng, Y. Yin, *Angew. Chem. Int. Ed.,* 2012, **51**, 5629-5633.
6. M. Chen, S. Tang, Z. Guo, X. Wang, S. Mo, X. Huang, G. Liu, N. Zheng, *Adv. Mater.*, 2014, **26**, 8210-8216.
7. Y. Xia, W. Li, C. Cobley, J. Chen, X. Xia, Q. Zhang, M. Yang, E. Cho, P. Brown, *Acc. Chem. Res*., 2011, **44**, 914-924.
8. F. Garćia-Vidal, J. Pendry, *Phys. Rev. Lett.*, 1996, **77**, 1163-1166.
9. S. Oldenburg, R. Averitt, S. Westcott, N. Halas, *Chem. Phys. Lett*., 1998, **288**, 243-247.
10. N. Halas, S. Lal, W. Chang, S. Link, P. Nordlander, *Chem. Rev.*, 2011, **111**, 3913-3961.
11. H. Wang, D. Brandl, P. Nordlander, N. Halas, *Acc. Chem. Res*., 2007, **40**, 53-62.
12. J. Millstone, S. Hurst, G. Métraux, J. Cutler, C. Mirkin, *Small*, 2009, **5**, 646-664.
13. M. Rycenga, C. Cobley, J. Zeng, W. Li, C. Moran, Q. Zhang, D. Qin, Y. Xia, *Chem. Rev.,* 2011, **111**, 3669-3712.
14. R. Jin, Y. Cao, C. Mirkin, K. Kelly, G. Schatz, J. Zheng, *Science,*2001, **294**, 1901-1903.
15. Y. Sun, Y. Xia, *Science*, 2002, **298**, 2176-2179.
16. X. Huang, S. Neretina, M. El-Sayed, *Adv. Mater.*, 2009, **21**, 4880-4910.
17. N. Li, P. Zhao, D. Astruc, *Angew. Chem. Int. Ed.,* 2014, **53**, 1756-1789.
18. Y. Xia, Y. Xiong, B. Lim and S. Skrabalak, *Angew. Chem., Int. Ed.*, 2009, **48**, 60-103.
19. N. Bastús, J. Comenge, V. Puntes, *Langmuir,* 2011, **27**, 11098-11105.
20. J. Gao, C. Bender, C. Murphy, *Langmuir*, 2003, **19**, 9065-9070.
21. F. Kim, J. Song, P. Yang, *J. Am. Chem. Soc.,* 2002, **124**, 14316-14317.
22. L. Chen, F. Ji, Y. Xu, L. He, Y. Mi, F. Bao, B. Sun, X. Zhang, Q. Zhang, *Nano Lett.*, 2014, **14**, 7201-7206.
23. L. Scarabelli, M. Coronado-Puchau, J. Giner-Casares, J. Langer, L. Liz-Marzan, *ACS Nano,*2014, **8**, 5833-5842.
24. R. Jin, S. Egusa, N. Scherer, *J. Am. Chem. Soc.*2004, **126**, 9900-9901.
25. J. Kim, S. Cha, K. Shin, J. Jho, J. Lee, *Adv. Mater*., 2004, **16**, 459-464.
26. J. Zhang, M. Langille, M. Personick, S. Li, C. Mirkin, *J. Am. Chem. Soc.*, 2010, **132**, 14012-14014.
27. W. Niu, Y. Chua, W. Zhang, H. Huang, X. Lu, *J. Am. Chem. Soc.,* 2015, **137**, 10460-10463.
28. M. Banaee, K. Crozier, *Opt. Lett.* 2010, **35**, 760-762.
29. E. Larsson, J. Alegret, M. Käll, D. Sutherland, *Nano Lett.* 2007, **7**, 1256-1263.
30. J. Aizpurua, P. Hanarp, D. Sutherland, M. Käll, G. Bryant, F. Abajo, *Phys. Rev. Lett*., 2003, **90**, 057401.
31. B. Wiley, S. Im, Z. Li, J. McLellan, A. Siekkinen, Y. Xia, *J. Phys. Chem. B,* 2006, **110**, 15666-15675.
32. A. Cetin, H. Altug, *ACS Nano*, 2012, **6**, 9989-9995.
33. M. Mahmoud, M. El-Sayed, *Nano Lett*., 2011, **11**, 946-953.
34. S. Skrabalak, J. Chen, Y. Sun, X. Lu, L. Au, C. Cobley, Y. Xia, *Acc. Chem. Res*., 2008, **41**, 1587-1595.
35. Y. Khalavka, J. Becker, C. Sönnichsen, *J. Am. Chem. Soc*., 2009, **131**, 1871-1875.
36. Y. Chen, H. Chen, L. Guo, Q. He, F. Chen, J. Zhou, J. Feng, J. Shi, *ACS Nano*, 2010, **4**, 529-539.
37. M. McEachran, D. Keogh, B. Pietrobon, N. Cathcart, I. Gourevich, N. Coombs, V. Kitaev, *J. Am. Chem. Soc.,*2011, **133**, 8066-8069.
38. F. Yan, W. Goedel, *Nano Lett*., 2004, **4**, 1193-1196.
39. T. Ozel, M. Ashley, G. Bourret, M. Ross, G. Schatz, C. Mirkin, *Nano Lett.*, 2015, **15**, 5273-5278.
40. W. Lai, J. Zhou, Z.Jia, L. Petti, P. Mormile, *J. Mater. Chem. C*, 2015, **3**, 9726-9733.
41. L. You, Y. Mao, J. Ge, *J. Phys. Chem. C,*2012, **116**, 10753-10759.
42. S. Scheeler, D. Lehr, E. Kley, C. Pacholski, *Chem. Asian J*., 2014, **9**, 2072-2076.
43. Y. Hu, T. Chou, H. Wang, H. Du, *J. Phys. Chem. C,* 2014, 118, 16011-16018.
44. Y. Sun, Y. Xia, *Adv. Mater*., 2003, **15**, 695-699.

45. G. Métraux, Y. Cao, R. Jin, C. Mirkin, *Nano Lett*., 2003, 3, 519-522.
46. C. Liusman, S. Li, X. Chen, W. Wei, H. Zhang, G. Schatz, F. Boey, C. Mirkin, *ACS Nano*, 2010, **4**, 7676-7682.
47. R. Near, C. Tabor, J. Duan, R. Pachter, M. El-Sayed, *Nano Lett.,* 2012, **12**, 2158-2164.
48. A. Halpern, R. Corn, *ACS Nano*, 2013, **7**, 1755-1762.
49. C. Tsai, J. Lin, C. Wu, P. Lin, T. Lu, P. Lee, *Nano Lett.*, 2012, **12**, 1648-1654.
50. H. Jang, S. Ham, J. Acapulco, J. Song, S. Hong, K. Shuford, S. Park, *J. Am. Chem. Soc*., 2014, **136**, 17674-17680.
51. Y. Li, Y. Yan, Y. Li, H. Zhang, D. Li, D. Yang, *CrystEngComm*, 2014, **17**, 1833-1839.
52. Y. Li, W. Wang, K. Xia, W. Zhang, Y. Jiang, Y. Zeng, H. Zhang, C. Jin, Z, Zhang, D. Yang, *Small,*2015, **11**, 4745-4751.
53. F. Fan, D. Liu, Y. Wu, S. Duan, Z. Xie, Z. Jiang, Z. Tian, *J. Am. Chem. Soc*., 2008, **130**, 6949-6951.
54. X. Huang, S. Tang, X. Mu, Y. Dai, G. Chen, Z. Zhou, F. Ruan, Z. Yang, N. Zheng, *Nat. Nanotech.*, 2011, **6**, 28-32.
55. X. Xia, S. Xie, M. Liu, H. Peng, N. Lu, J. Wang, M. Kim, Y. Xia, *P. Natl. Acad. Sci. USA*, 2013, **110**, 6669-6673.

Nanoscale Accepted Manuscript